Planetary and Space Science 69 (2012) 18–27

Contents lists available at SciVerse ScienceDirect

Planetary and Space Science

journal homepage: www.elsevier.com/locate/pss

Confirmation of sublunarean voids and thin layering in mare deposits

M.S. Robinson [a,*], J.W. Ashley [a], A.K. Boyd [a], R.V. Wagner [a], E.J. Speyerer [a], B. Ray Hawke [b], H. Hiesinger [c,d], C.H. van der Bogert [c]

[a] School of Earth and Space Exploration, Arizona State University, Tempe, AZ, USA
[b] Hawaii Institute of Geophysics and Planetology, School of Ocean and Earth Science and Technology, University of Hawaii, Honolulu, HI, USA
[c] Institut für Planetologie, Westfälische Wilhelms-Universität, Münster, Germany
[d] Brown University, Providence, RI, USA

ARTICLE INFO

Article history:
Received 6 February 2012
Received in revised form
16 May 2012
Accepted 16 May 2012
Available online 26 May 2012

Keywords:
Moon
Volcanism
Impact melt
Shelter
Pit
Flow

ABSTRACT

Typical flow thicknesses of lunar mare basalts were not well constrained in the past, because as craters and rilles age, downslope movement of loose material tends to mix and bury stratigraphy, obscuring the three dimensional nature of the maria. New Lunar Reconnaissance Orbiter Camera high resolution images unambiguously reveal thicknesses of mare basalt layers exposed in impact craters, rilles, and steep-walled pits. Pits up to one hundred meters deep present relatively unmodified, near-vertical sections of mare in three cases, and many young impact craters also expose well preserved sections of mare. Oblique views of each pit and many of these craters reveal multiple layers, 3 to 14 m thick, indicating that eruptions typically produced a series of ~10 m thick flows (or flow lobes) rather than flows many tens to hundreds of meters thick. Additionally, these images unambiguously show that the floors of two pits extend beneath the mare surfaces, thus revealing sublunarean voids of unknown lateral extent. We also document the occurrence of pits that may be expressions of collapse into subsurface voids in non-mare impact melt deposits. These voids are compelling targets for future human and robotic exploration, with potential as temporary shelters, habitations, or geologic museums.

1. Introduction

The existence of sublunarean voids was hypothesized as far back as 1885 (e.g., Nasmyth and Carpenter, 1885; Coggins and Pratt, 1952; Halliday, 1966; Heacock et al., 1966; Hatheway and Herring, 1970; Hörz, 1985; Coombs and Hawke, 1992). After the discovery and quantification of the radiation environment in cis-lunar space (Hörz, 1985), it was realized that geologic features such as locally collapsed lava tubes (skylights) could provide access to shelters from radiation and other surface hazards (Hörz, 1985; Coombs and Hawke, 1992; De Angelis et al., 2002). The first steep-walled lunar pits were identified in SELenological and ENgineering Explorer (SELENE) Terrain Camera (TC) images (Haruyama et al., 2009, 2010) (Appendix A). The first-discovered pit is located (Fig. 1) in the Marius Hills region of Oceanus Procellarum (14.1°N, 303.2°E) (Haruyama et al., 2009). The two other pits were found within Mare Tranquillitatis (8.3°N, 33.2°E) and Mare Ingenii (36.0°S, 166.1°E) (Haruyama et al., 2010). More than 150 additional pits, of various shapes and sizes, are identified in Lunar Reconnaissance Orbiter Camera (LROC) Narrow Angle Camera (NAC) (Robinson et al., 2010) images associated with impact melt deposits within 21 craters.

1.1. Terminology

The term 'pit crater' can refer to several types of landforms with different formation mechanisms, terrestrial pit craters are typically characterized by circular to oblate outlines, near-vertical walls, a lack of overflow or ejecta on their rims, and an association with volcanic deposits and processes (e.g., Carr and Greeley, 1980; Okubo and Martel, 1998; Howard, 2010). On Earth, pit crater environments include collapsed roofs of small magma chambers or broad cavities, partially drained dikes, and piston-like ground subsidence areas over rift zone fractures (e.g., Carr and Greeley, 1980). Terrestrial pit craters are usually defined as the surface expression of stoping through ceilings of underlying void spaces with eventual surface collapse (Okubo and Martel, 1998; Howard, 2010).

The morphologic characteristics of the three largest steep-walled lunar pits described here are consistent with the terrestrial examples mentioned above. However, enough confusion persists over the precise definition of the term 'pit crater' to avoid its use when describing pits that may be lava tube skylights (e.g., Cushing et al., 2007, Halliday 1998, 2008). Though exceptions have been noted, the genetic similarity between lava tube

* Corresponding author. Tel.: +1 4807279691.
E-mail address: mrobinson@asu.edu (M.S. Robinson).

0032-0633/$ - see front matter © 2012 Elsevier Ltd. All rights reserved.
http://dx.doi.org/10.1016/j.pss.2012.05.008

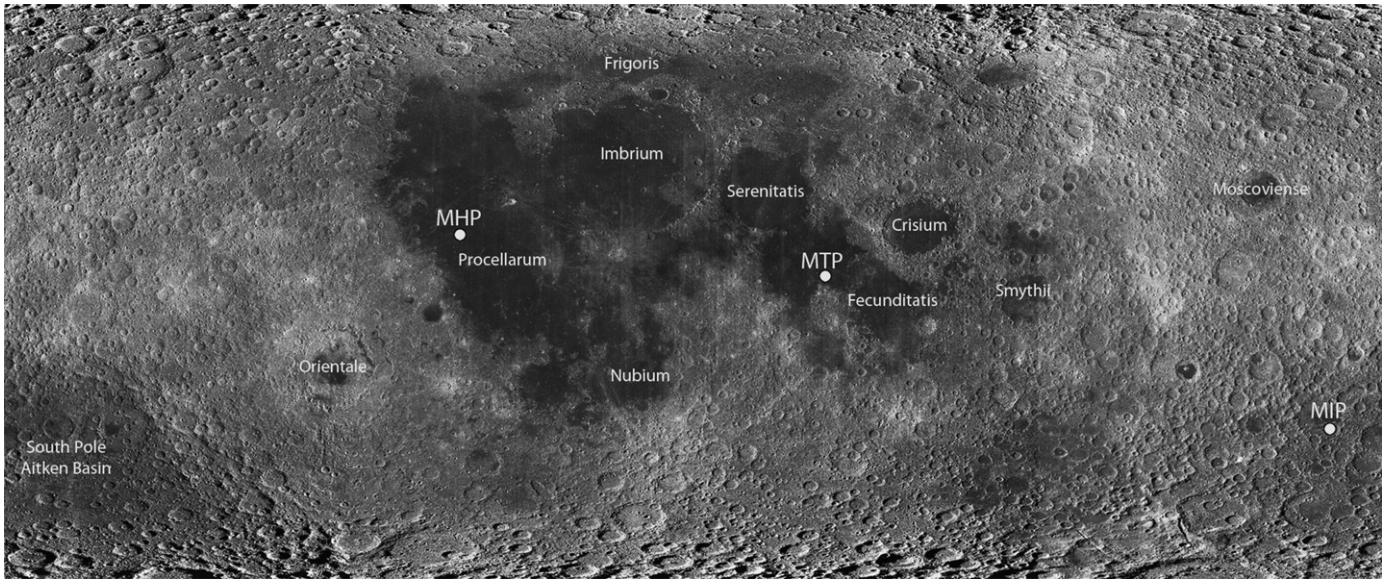

Fig. 1. LROC WAC mosaic showing locations of the three steep walled mare pits, area covers 180 °W to 180 °E longitude, and ± 75° latitude. MHP Marius Hills Pit (14.091 °N, 303.223 °E), MTP Mare Tranquillitatis Pit (8.335 °N, 33.222 °E), MIP Mare Ingenii Pit (35.950 °S; 166.057 °E).

Table 1
Feature dimensions with LROC derived coordinates.

Feature region (mare or melt pond)	Diameter (m)	Depth* (m)	Location	
			Lat	Long
Ingenii	103, 66	37–63	35.950 °S	166.057 °E
Tranquillitatis	99, 84	107	8.335 °N	33.222 °E
Marius Hills	57, 48	45	14.091 °N	303.233 °E
King pond bridge	56, 24	11	6.241 °N	119.735 °E
Copernicus pond pit	90, 50	23	10.329 °N	339.619 °E

Note: Pit diameters are presented as maximum and minimum.

* Presented depths were measured from the sharp break in slope to the pit floor. Depths are calculated from shadow measurements.

skylights and classic magma chamber pit craters is described as '*limited*' (Halliday, 1998), with this author calling for a redefinition of pit crater that precludes its confusion with skylights.

Moreover, while the Marius Hills pit is plausibly proposed to be a skylight based on its location within a sinuous rille (Haruyama et al., 2009), less certainty exists for the origin of the Tranquillitatis and Ingenii pits, both located in relative isolation from obvious rille systems. Tectonic features are common in the maria and may play a direct or indirect role in pit formation. Imaging of cavernous interiors extending under a mare (or direct exploration by a landed element) would certainly clarify the origin of the main pit features discussed below. However, until more is known about the formation mechanisms of these mare pits, we adopt the term 'steep walled pit', or simply 'pit' for brevity.

2. Pit morphology

The NAC images allow detailed topographic and morphologic descriptions of the three mare pits (Fig. 1), giving insight to their origin and significance (Table 1, Appendix A). In the following sections each pit and its local environment are described.

2.1. Mare Ingenii pit

Mare Ingenii embays Thomson (115 km diameter), Thomson M (110 km diameter) and the surrounds, and is one of the larger farside mare deposits. Mare Ingenii is perhaps most notable for the distinctive swirl patterns that superpose its surface (Hood et al., 1979, Blewett et al., 2011, Kramer et al., 2011). The Ingenii pit is near the center of the crater Thomson *M*, ~10 km west of a knobby region, indicating the mare may be thin in this area. Close to the pit are no distinguishing tectonic or mare flow features: the immediate surrounding mare surface is most notable for their lack of distinguishing features.

The Mare Ingenii pit was imaged by the NAC 13 times with incidence angles (intersection of solar vector measured from the surface normal) ranging from 35° to 82° (Fig. 2). The pit has an ovoid outline with a long axis aligned approximately north–northeast to south–southwest (Fig. 3). Measured from the sharp break in slope along the perimeter, maximum and minimum pit diameters are 104 m and 71 m. Depths from shadow measurements range from ~64 m at the south–southwest end to ~39 m at the north–northeast end (these measurements are from where the shadow is cast, which is below the level of the surrounding mare). The variable depths result from a sloping talus field that covers much of the pit floor, which may also partially (or completely) obstruct any potential cavern entrance. Depths from shadow estimates are point measurements by nature, and may not fully capture the range of depths from the rim, or fully describe floor roughness. Additionally, a shadow measurement represents depth from the point where the pit slope exceeds the complement of the incidence angle, which is below the level of the surrounding mare surface (there is a shallow, sloping apron surrounding each pit). Depths measured with stereogrammetric techniques (Tran et al., 2010) (M123485893R, M138819477R) range from ~38 to ~67 m in the same points as the shadow measurements (measured from the lip below the surrounding plain confirming the shadow measurements). The maximum depth below the surrounding mare to the pit floor is ~87 m. The pit walls exhibit five measureable layers; from top to bottom their thicknesses are 5, 6, 7, 11, and 8 ± 1 m, respectively. We assume that talus covers the bottom of each layer and does not hide thinner layers.

Block diameters on the pit floor range from 1 m (the smallest detectable size) to 5 m, with the largest fragments clustered at the west (M128202846L) and southwest (M123485893R) ends of the floor. The standard deviation of reflectance values of the west–southwest floor is seven times that of the surrounding mare

surface, while the east–northeast floor reflectance standard deviation is three times as high as the mare (M123485893R), indicating that the entire floor is rougher than the surrounding mare surface. No impact craters are identifiable on the pit floor.

2.2. Mare Tranquillitatis pit

The Mare Tranquillitatis pit is not co-located with rilles, domes, or tectonic features (Figs. 1 and 4), but rather located in a rather unexceptional expanse of mare. The closest major landform is a chain of secondary craters (Wilhelms, 1972) located ~3 km west–northwest of the pit. The Tranquillitatis pit is also within 70 km of two closed depressions (small white arrows, Fig. 4) that are associated with the Rupes Cauchy rille structure. As Rupes Cauchy is interpreted to be a graben structure (Wilhelms, 1972), there may be local tectonic stresses that contributed to the formation of this pit.

This pit was imaged by the NAC 10 times with incidence angles ranging from 11° to 48°, and a maximum emission angle (intersection of the camera boresight measured from the surface normal) of 51°. Pit diameters range from 86 to 100 m, with a maximum depth from shadow measures of ~107 m (Fig. 5A, B).

An oblique view (26° emission angle) of the pit in Mare Tranquillitatis shows ~20 m of floor extending beneath a ceiling, thus confirming a sublunarean void (Fig. 5D). Subtracting the thickness of the visible ledge (~47 m) from the depth of the pit indicates the void space to be ~60 m high. Since oblique imaging cannot provide a view of ceiling heights beyond the immediate pit perimeter, it is unknown whether ceiling heights increase or decrease further into the void (Fig. 6). The oblique images (Fig. 5D and E) also emphasizes a conspicuous funnel-shaped slope at the rim, and reveals layering in the walls. Thicknesses of the layers (including talus) range from 3 to 14 ± 1 m (Fig. 5F).

Several large, angular blocks, ranging in size from 3 to 8 m are sparsely distributed across the floor, and likely represent detritus from the pit walls or collapsed roof materials (Fig. 5). The standard deviation of the integrated floor reflectance is five times that of the surrounding mare, while the smooth area between the boulders is only 1.8 times higher (M12348593R).

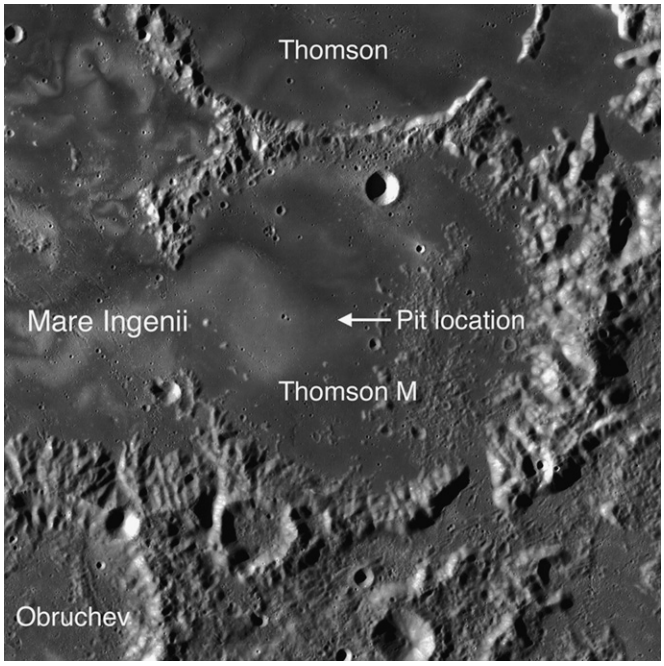

Fig. 2. Mare Ingenii pit context map (LROC WAC mosaic), orthographic projection centered at 36.0 °S latitude and 166.1 °E longitude, map width 186.2 km, north is up.

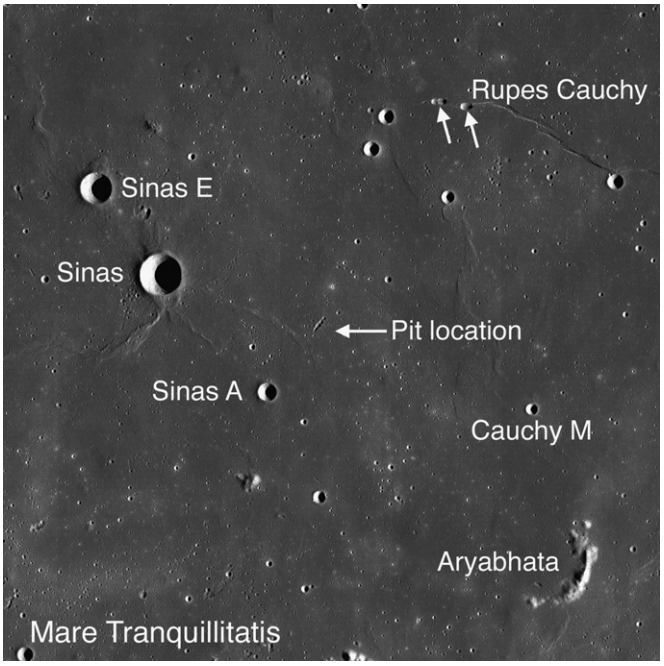

Fig. 4. Mare Tranquillitatis pit context map (LROC WAC mosaic), orthographic projection centered at 8.3°N latitude and 33.2°E longitude, map width 183.2 km, north is up.

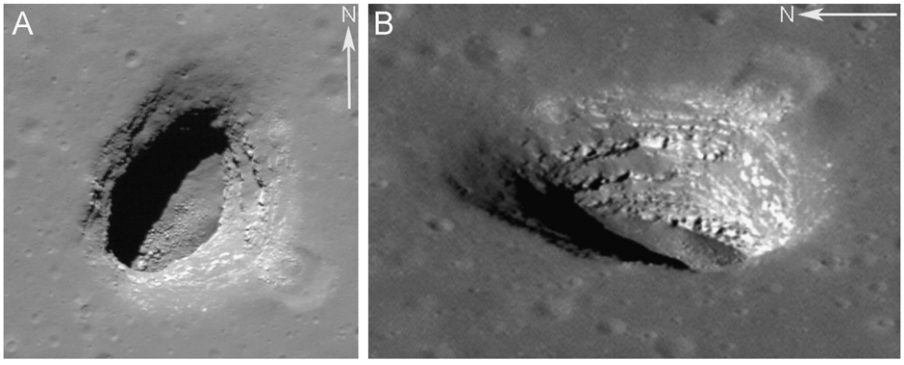

Fig. 3. (A) Mare Ingenii pit seen with a 7° emission angle and 39° incidence angle (M123485893R), image is approximately 220 m wide. (B) Oblique view with 43° emission angle acquired looking from west to east downsun (44° incidence angle; M184810930L).

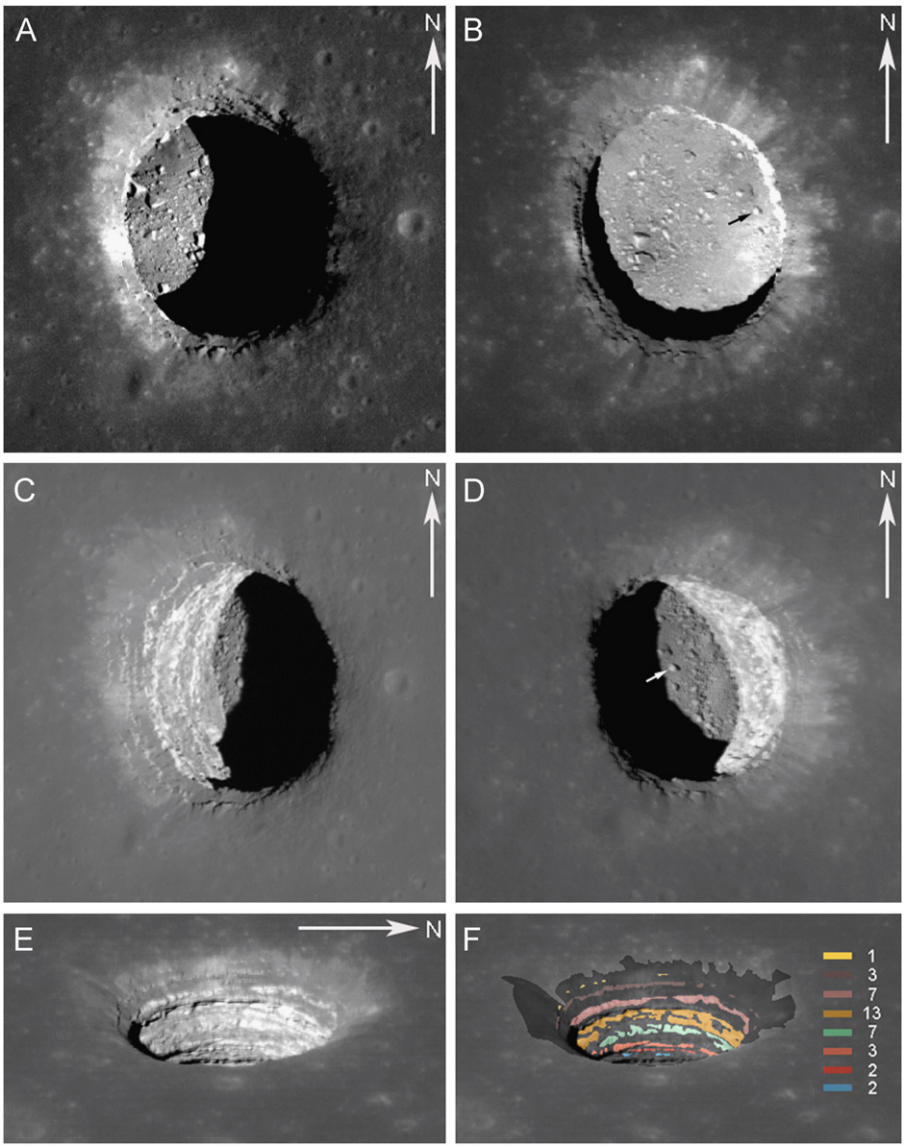

Fig. 5. Mare Tranquillitatis pit in two near-nadir images (Table A1) with opposite Sun azimuth angles: (A) M126710873R and (B) M155016845R. Together these two images reveal more than 90 percent of the pit floor, both images are approximately 175 m wide. Oblique views: (C) layering in west wall and a portion of pit floor beneath overhanging mare (29° emission angle; M175057326R); (D) A significant portion of the illuminated area is beneath the eastern overhanging mare in this image (26° emission angle; M152662021R), white arrow indicates same boulder marked with black arrow in panel B. Detailed layering is revealed in (E) and (F) (M155023632R and M144395745L, respectively). Outcropping bedrock layer thickness estimates are presented in (F) in meters, ± 1 m.

2.3. *Marius Hills pit*

The Marius Hills pit is located in a sharp bend of a shallow east-to-west trending rille (Haruyama et al., 2009), approximately 32 km downslope from its distinctive pit vent. The host rille cuts a pre-existing wrinkle ridge (250 m relief on its western side), which in the area of the pit is ~500 m wide and exhibits about 25 m of relief. Within 25 km of the pit there are at least 10 domes (volcanic structures) (Karlstrom et al., 1968; Whitford-Stark and Head, 1977) that are on the northwest flank of a broad rise (250 km diameter, 1500 m maximum relief) proposed to have formed as a shield volcano (Spudis et al., 2011). Of the three large pits discussed here, the Marius Hills example is in the most complicated volcanic–tectonic terrain.

The NAC imaged the Marius Hills pit (Fig. 7) seven times under a variety of lighting conditions (incidence angles ranged from 13° to 83° (Fig. 8)). The pit outline is slightly elliptical, with diameters ranging from 49 to 57 m (Appendix A; Fig. 8). From the southwest rim to one third of the floor diameter (from southwest to northeast), shadow measurements show a maximum depth of 43 ± 2 m (M122584310L). Haruyama et al., 2009 also used shadow measurements on 10 m/pixel SELENE TC data to estimate Marius Hills pit depths of 80 to 90 m. Photogrammetric techniques (Tran et al., 2010) from a NAC stereo pair (M155607349, M155614137) confirmed the NAC shadow measurements. Our stereo-derived digital terrain model shows the pit floor to be 40 to 44 m below the sharp rim and 51 m below the surrounding flat mare surface.

An oblique (43° emission angle) NAC image that was closely aligned with the incidence vector captured illuminated portions of the pit floor beyond the nadir-view pit perimeter, and beneath ceiling rock, revealing a sublunarean void (Fig. 8). The distance imaged along the floor into the cavern (beneath the ceiling) is ~12 m, and the height of the ceiling above the floor is ~17 m; whether the void extends beyond the shadow edge is unknown. This oblique image also reveals eight layers in the pit wall that range in thickness from 4 to 12 ± 1 m, with an average thickness of 6 m (assuming talus does not obscure thinner layering at the base of layers).

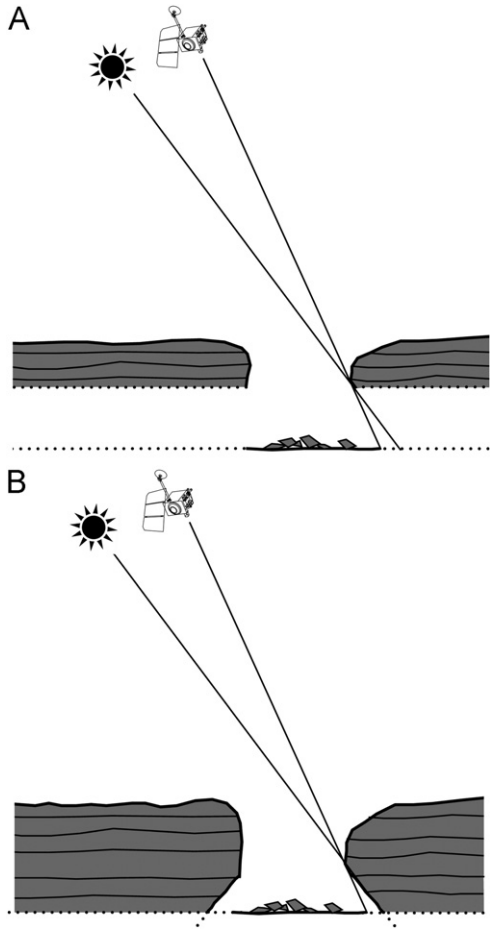

Fig. 6. Model of pit formation as (A) collapse into lava tube (skylight), and (B) collapse into near surface magma chamber resulting in an inverted cone shaped void. Dashed lines are speculative in both scenarios.

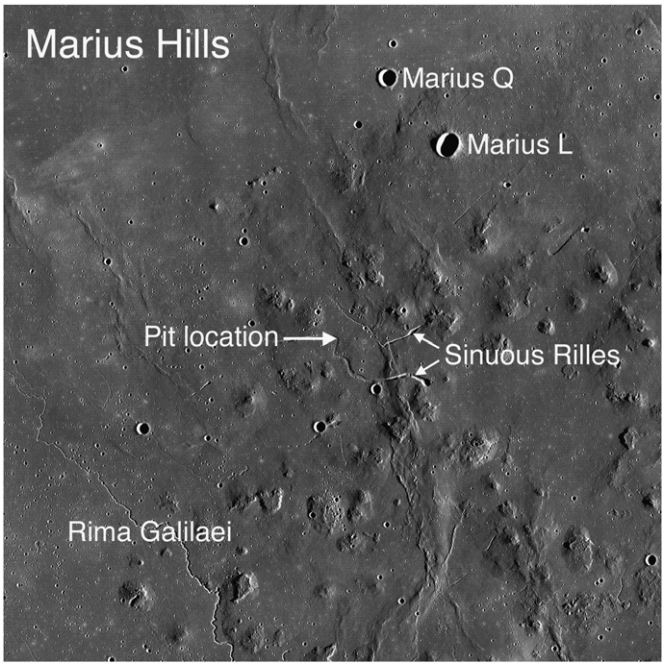

Fig. 7. Marius Hills pit location map (LROC WAC mosaic), orthographic projection centered at 14.1°N latitude and 303.2 °E longitude, map width 184.1 km, north is up. The many irregular positive relief features in the east and south portions of the mosaic are the Marius Hills domes.

The floor of the Marius Hills pit is littered with meter-scale blocks and no resolvable impact craters. Forty-six of ninety-three blocks measured within the illuminated area are larger than 2 m, with the largest block having a maximum length of 5 m. The standard deviation of reflectance values of the pit floor is five times higher than that of the reflectance of the surrounding mare, indicating a blockier surface (M122584310L).

2.4. Thickness of mare flows

Understanding the types and expressions of lunar volcanism is a fundamental topic of lunar research (BVSP, 1981). Establishing the presence and character of layering within mare deposits has significance for investigating basalt flow effusion mechanisms, cooling history, and regolith development between flows. Chief among the questions relating to mare emplacement is how many separate flows occurred at given locations in the mare basins, how voluminous they were, and over what time scale they were emplaced (Hiesinger et al., 2003, 2011; Head and Wilson, 1992; Schaber et al., 1976; Shearer et al., 2006). Thickness and volume estimates for basin deposits were originally based on assumptions that basin filling occurred either during massive events with a small number of more-or-less contemporaneous flows, or as fractionated lava lake deposits (O'Hara et al., 1970; Biggar et al., 1971).

Evidence for multiple, relatively thin mare flows was documented by the Apollo 15 reconnaissance of Hadley Rille in 1971 with the observation of layers 10 to 20 m thick (Howard and Head, 1972; Spudis et al., 1988). Inspection of a complete cross-section was made difficult, however, by talus covering most of the rille wall; thus the precise number of individual layers and their thicknesses could not be accurately measured. Howard and Head (1972) speculated that the thinnest of these layers (1) were each the result of separate eruption events, (2) were the result of multiple flows from a single eruption, or (3) represent eroded vesicle-rich zones. Because Hadley Rille runs along the western Apennine Mountain front, skirting the margins of Palus Putredinis/Mare Imbrium, it is also possible that the thin units result from a margin thinning effect, and are not representative of actual flow thicknesses in the basin interior (Howard and Head, 1972).

Subsequently, the concept of multiple flow events was proposed for Mare Imbrium (Whitaker, 1972; Schaber, 1973), Mare Serenitatis (Sharpton and Head, 1982; Weider et al., 2010), Oceanus Procellarum (Weider et al., 2010), and other mare basins (Head, 1976). Schaber et al. (1976) suggested that compound flow units are the result of multiple (but temporally related), low-rate effusion events close (within 120 km) to their source vent. They further suggested that compound units were the most common form of basalt emplacement in lunar maria. Evidence for thin flows (<10 m) is provided by flow front shadow measurements for late-stage *surface* units (Lloyd and Head, 1972; Gifford and El-Baz, 1981), and also inferred from chemical kinetic studies of Apollo samples (Brett, 1975; Kubo et al., 2010). Distinctive kinks in crater size-frequency distributions measured for several mare basins were used to estimate the thickness of individual flows to be on the order of 30 to 60 m on average (Hiesinger et al., 2002).

Compositional studies based on impact excavations into mare stratigraphy (using ejecta and/or crater wall interiors) yield thicker individual flow estimates (100 to 300 m) for the Marius Hills region of Oceanus Procellarum, and 80 to 600 m for Mare Serenitatis (Weider et al., 2010). This method relies on differences in composition from flow-to-flow to mark flow thickness, and thus is insensitive to flow layering that is compositionally homogeneous. Indeed, these estimates likely represent thicknesses of multiple individual flows (or flow lobes) of the same composition rather than single massive flows. Thick ($>$ 50 m) surface flows

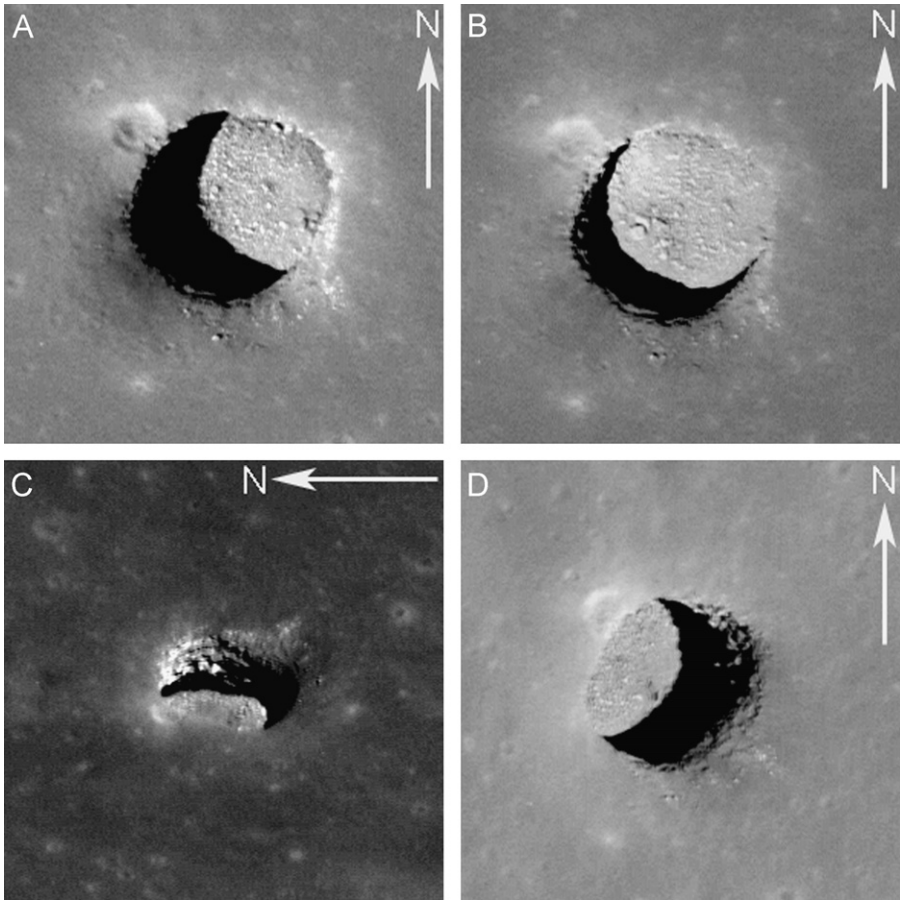

Fig. 8. Marius Hills pit in a (A) near-nadir (0.5° emission angle) image (M122584310L) showing pit outline and rubble-strewn floor (25° incidence angle); image is approximately 140 m wide. (B) M155607349R shows even more of the illuminated floor with emission angle 9°; incidence angle is 13°. (C) M137929856R (34° incidence angle and a 45° emission angle) shows ~12 m of illuminated floor beneath the cavern ceiling. Note layering in pit walls; image is approximately 250 m wide. (D) M155614137R (30° emission angle) with eastern wall in shadow; incidence angle is 13°.

are rare but not unexpected on the Moon (e.g., those detected within the Mare Imbrium flow field (Gifford and El-Baz, 1981; Masursky et al., 1978)). Such flows are easily explained as 'last gasp' effusions from a nearly expended magma source.

The thin layering (3 to 14 m) revealed in the NAC images of the Marius Hills, Tranquillitatis, and Ingenii pit walls provide evidence in cross-section for flow thicknesses in mare deposits from around the Moon. Because each pit location is well removed from its respective mare margin, the deposits are representative of true mare flow thicknesses, and are not the product of any marginal thinning effects. Meter to decameter layering in each of the three steep-walled pits could mean either that (1) there is a genetic relationship between pit occurrence and layering, or that (2) thin flows were widespread on the Moon. The occurrence of thin surface flow units seen elsewhere on the Moon (e.g., Gifford and El-Baz, 1981), and the significant number of thin layers exposed in the pit walls, are consistent with the second hypothesis. In addition, NAC imagery has revealed thin layers in the walls of at least 12 impact craters in the mare. Typical examples are represented by Bessel crater (21.94°N, 18.04°E) in Mare Serenitatis, and Kepler (7.66°N, 322.09°E) in Oceanus Procellarum (Fig. 9). While it is possible that processes that formed the pits somehow resulted in anomalously thin layering at each pit, we note that at Hadley rille and in many of these mare crater walls, horizontal layering is exposed for hundreds of meters horizontally and vertically. Thus it is probable that the layers exposed in the pits and crater walls are representative of the average thickness of flows (or flow lobes) across broad areas of all mare.

3. Origin and significance of sublunarean voids

The lack of raised rims, ejecta fields, steep wall slopes, and depth-to-diameter ratios of the pits preclude an exclusively impact-related origin (although collapse into an underlying void may have been initiated by an impact event). Haruyama et al., 2009, 2010 proposed that the pits formed as roof collapse into lava tubes (skylights). The subsurface voids discovered with NAC oblique imaging raises the distinct possibility of extensive open lava tube systems. Alternately, the pits could represent collapse events into voids created as magma drained from near surface chambers: inverted funnel shaped pits are known from terrestrial examples (Halliday, 1998). Since the NACs can only image a few tens of meters under the overhangs, it is not possible to definitively discriminate between the two formation mechanisms at this time (Fig. 6).

No impact craters are resolved in any of the three major mare pits, an observation consistent with a young age. However material falling from the steep walls to the floor may rapidly obscure any craters that may have formed. Additionally, steep walls shield the floor from bolides coming in at oblique angles. A more compelling argument for a relatively young age for the pits is simply their presence. Since the estimated lifetime of a 100 m diameter crater on the Moon is roughly 100 million years (Gault, 1970) it is likely that pits are younger than that age, and that the pits formed well after their host mare were emplaced.

Any long-term human presence on the Moon requires reliable protection from surface hazards (radiation, micrometeoroids,

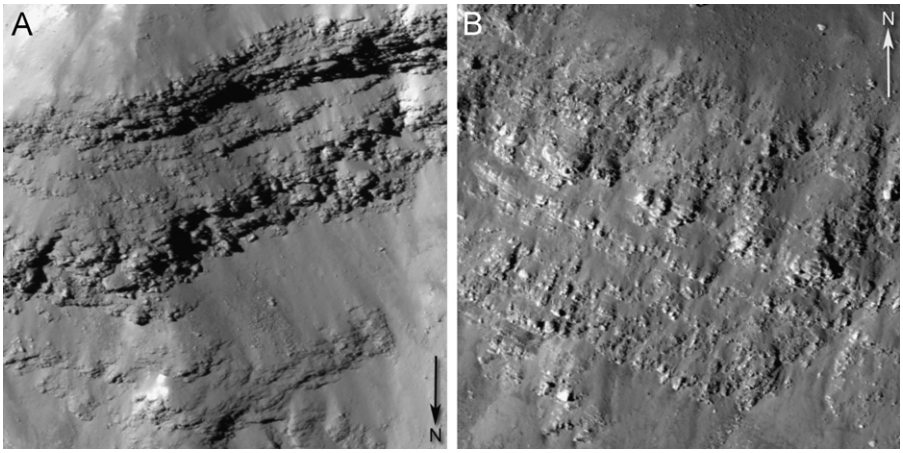

Fig. 9. Horizontal striations visible in crater walls indicate mare flow thicknesses of 2 to 5 m. (A) Kepler crater (M111843702L; 33° incidence angle, 1° emission angle); (B) Bessel crater (M135073175R; 64° incidence angle, 0° emission angle). Each image is ~300 m wide. Striations are visible through ~400 m of vertical section in both images.

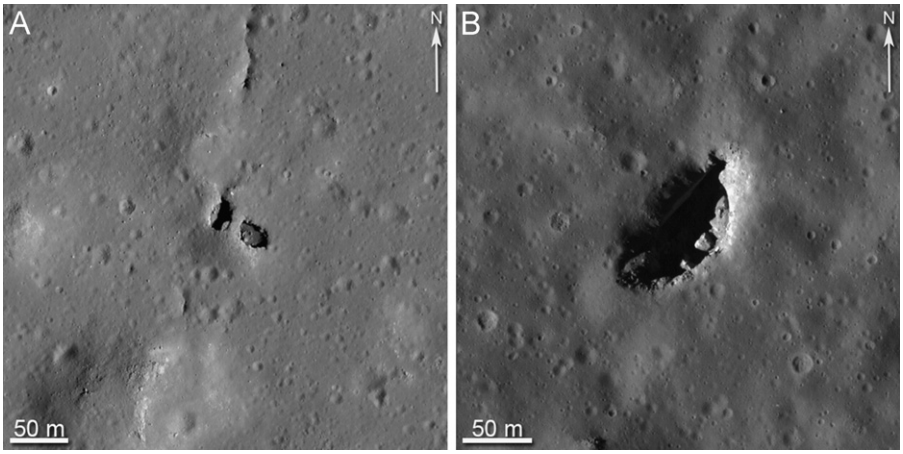

Fig. 10. (A) Rock bridge traversing a subsurface void in large impact melt pond north–northwest of King crater (M113168034R; 48° incidence angle, 1° emission angle); image is 387 m wide. (B) Pit (approximately 20 m deep) in Copernicus crater melt deposit (M135317661R; 58° incidence angle, 17° emission angle); image is 324 m wide.

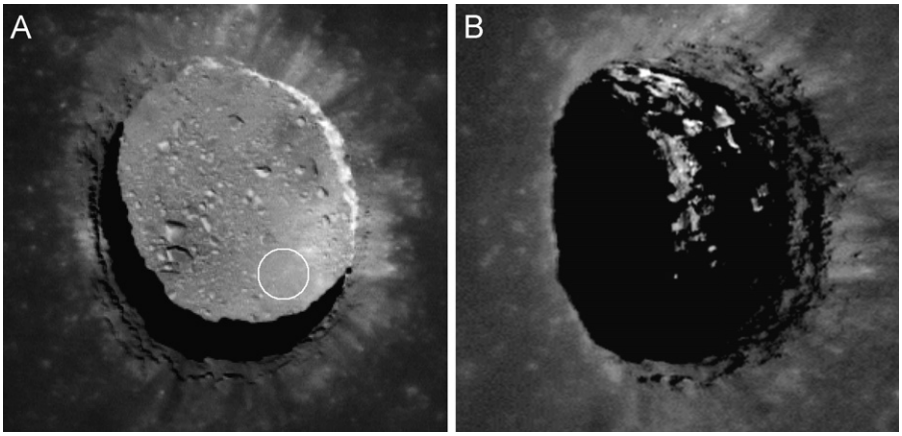

Fig. 11. (A) Expanded view (2 × enlargement) of Mare Tranquillitatis pit, circle indicates 16-m diameter proposed landing site (M155016845R), image is 298 m wide. (B) Oblique view (M155023632R, 42° emission angle) of same pit acquired on next orbit (~2 h later) looking from west to east. Note that no portion of the floor is visible, despite the fact that the Sun is behind the spacecraft and nearly the whole floor is illuminated—much of the large shadowed region is under the mare.

temperature cycling), which can be accomplished effectively using extant caverns (Hörz, 1985; Coombs and Hawke, 1992; De Angelis et al., 2002; Haruyama et al., 2009). In addition to the three steep-walled pits detailed here, LROC NAC images have revealed over 150 additional pits formed in impact melt deposits (Appendix B), with the largest (70 to 100 m diameter) found associated with Crookes and Copernicus craters (Fig. 10). These pits likely are the result of collapse into subsurface voids, possibly into a tube system formed by subsurface movement of melt. As with the mare examples, it is unknown whether the impact melt pits represent openings to intricate plumbing networks, possibly extending for hundreds of meters or even more.

Extant lava tubes could expose a diversity of pristine geologic formations: (1) delicate sublimate minerals, (2) paleo-regolith between basalt layers, possibly harboring ancient samples of solar wind, (3) unambiguous records of compositional evolution of magma source regions (e.g., Weider et al., 2010; Crawford et al., 2007), and/or (4) surface flow morphologies. There are likely other smaller mare pits to be discovered as the NACs continue to image the Moon. A small pit (13 to 17 m diameters) was recently located in Mare Smythii (2.702°S, 86.780°E; M119285915R), and like its larger antecedents may offer access to another sublunarean void in a different mare.

Could a robotic (or crewed) vehicle safely land within one of the three large mare pits? The NAC images of the pit floors show them to be rougher than the surrounding mare surface at the pixel scale. Since the floors are mostly shielded from micrometeoroid bombardment, and the walls serve as a source of blocks, this enhanced roughness is not unexpected. Landing hazards in the form of boulders >50 cm are visible on the floors of all three, however each pit floor has regions that are relatively smooth at the sub-meter scale. With the available data (due to the relatively high latitude (36°S) of the Ingenii pit, much of its floor remains unilluminated in the NAC images), the best candidate landing site is on the floor of the Tranquillitatis pit. Here, there is a relatively smooth area on the southeast portion of the floor with a diameter approaching 20 m (Fig. 11). Within the circle (Fig. 11) there are no resolvable blocks and the standard deviation of reflectance values approaches that of the surrounding mare (0.002 and 0.001, respectively), thus any blocks are of <50 cm size range. Safely landing on a small target within a pit requires precise navigation and a real-time hazard avoidance system. Once on the floor it is not known what obstacles such an intrepid explorer might find in the sublunarean voids, but the potential payoff is high.

Acknowledgements

The authors wish to thank Drs. Sonia Calvari and Lazlo Keszthelyi for insightful critiques and comments on an early version of this work and a helpful review by D. Blewett. NASA's Lunar Reconnaissance Orbiter project funded much of this work. Hiesinger and van der Bogert were supported by the Deutsches Zentrum für Luft-und Raumfahrt.

Appendix A

See Table A1.

Appendix B

See Table B1.

Table A1
Pit dimensions and narrow Angle Camera imaging parameters. Pit depths indicated are based on shadow length measurements with an accuracy that varies with scale, but which is generally better than ± 5 m. Slew, incidence, and emission angles are measured from the surface normal. Slant distances are measured along a direct line of sight from the camera to the center of each target.

Target	Image	Shadow length	Depth	Diameter		Slew angle*	Incidence angle	Emission angle	Phase angle†	Slant distance	Average pixel scale
				Max	Min						
		(m)	(m)	(m)	(m)	(°)	(°)	(°)	(°)	(km)	(m/pix)
Mare Tranquillitatis pit	M106662246R	62	105	100	86	0.00	30.37	1.38	29.04	134.06	1.34
8.335 °N; 33.222 °E	M126710873R	54	108	99	88	0.00	26.48	0.48	26.04	41.30	0.41
	M137332905R	59	78	102	88	7.05	37.28	7.18	30.31	46.75	0.47
	M144395745L	NA	NA	101	NA	−50.46	47.92	51.39	8.12	70.75	0.71
	M152655237R	NA	NA	100	NA	18.28	35.84	17.89	53.54	42.02	0.42
	M152662021R	NA	NA	100	NA	−24.41	36.78	25.85	11.92	44.16	0.44
	M155016845R	14	72	99	83	−3.61	10.57	5.22	7.31	40.70	0.41
	M155023632R	NA	NA	104	NA	−39.25	11.32	41.82	33.36	53.70	0.54
	M175057326R	NA	NA	98	NA	−28.00	41.62	28.50	14.75	26.89	0.27
	M188021351R	29	97	101	86	2.00	16.60	3.68	13.34	115.72	1.15
Marius Hills pit	M114328462R	NA	NA	59	NA	6.80	61.39	6.39	67.71	47.06	0.47
14.091 °N;	M122584310L	19	40	58	49	0.00	25.15	0.48	25.57	43.47	0.43
303.223 °E	M133207316L	NA	NA	NA	NA	29.13	82.85	27.95	54.92	52.75	0.53
	M137929856R	NA	NA	NA	47	42.86	33.81	44.89	18.86	65.07	0.65
	M150904816L	NA	NA	NA	NA	−54.70	59.52	54.52	8.86	70.47	0.70
	M155607349R	10	45	55	51	8.81	12.63	8.81	15.86	43.14	0.43
	M155614137R	NA	NA	NA	49	30.15	12.75	30.15	30.66	48.95	0.49
Mare Ingenii pit	M115225180L	NA	NA	NA	NA	0.00	74.38	2.00	76.34	68.05	1.02
35.950 °S; 166.057 °E	M121124338L	NA	NA	103	NA	0.00	51.98	2.48	53.97	56.58	0.57
	M123485893R	44	54**	106	70	−5.45	39.04	6.71	37.47	56.29	0.56
	M128202846L	NA	NA	NA	NA	0.00	54.14	1.10	55.06	56.77	0.57
	M136465172L	NA	NA	NA	NA	15.51	55.37	15.81	41.96	71.00	0.71
	M138819477R	52	64**	103	72	0.00	38.80	0.72	38.50	68.43	0.68
	M145896212L	NA	NA	NA	NA	0.00	68.29	0.94	69.19	68.49	0.69
	M171835900L	40	58**	104	70	0.08	34.58	0.44	34.55	68.98	0.69
	M180078882L	NA	NA	NA	NA	−0.01	81.63	2.11	**83.74**	**72.73**	**1.09**
	M182437764R	**NA**	**NA**	**NA**	**NA**	0.00	**60.30**	**2.49**	**58.09**	**72.38**	**0.72**
	M184810930L	NA	NA	NA	NA	−41.49	44.21	42.65	**35.66**	**96.11**	0.96
	M184789489R	**NA**	**NA**	**100**	**68**	15.47	**42.79**	**14.96**	**52.63**	**74.47**	0.74
	M184796637R	**43**	**76****	**102**	**67**	−5.68	**43.25**	**7.12**	**39.50**	**72.49**	0.72

NA = not applicable (measurements prohibited by viewing geometry).

* Defined as positive when slewing east, negative when slewing west.

** Greatest depth; see Section 2.1.

† Defined as the angular separation between the solar incidence vector and the emission vector.

Table B1
Impact melt pits. Numbers do not necessarily represent comprehensive tallies.

Crater Name	Image containing largest pit	Number of identified pits > 5 m wide	Maximum diameter (m)	Approximate depth of largest pit (m)
Adams B	M126499815R	3	17	5
Aristarchus	M109548636L	13	23	5
Aristillus	M111592038R	4	28	20
Copernicus	M135317661R	20	100 × 45*	25
Crookes	M110316458R	11	70 × 30*	< 15†
Harriot	M123826391L	1	30	10
Hayn	M154705713R	1	20	5
Jackson	M125645661L	7	25	20
Kepler	M111843702L	4	50	20
King	M113168034R	50	55	10
Klute W	M140840176R	4	20	10
Lalande	M114009947R	12	20	5
Messier A	M126622485R	2	33	15
Ohm	M125313001R	2	20	< 20†
Palitzsch B	M170118311R	1	14	10
Picard	M134829026R	1	15	5
Proclus	M170253317R	2	40	10
Runge	M119285915R	1	17	5
Rutherfurd	M109305653L	2	23	5
Stefan L	M158307753L	1	34	10
Stevinus	M124212055L	15	55	20
Virtanen	M156435317L	1	28	15

* Maximum and minimum diameters differ by more than 50 percent (both diameters are given).

† Slew angles range from 8° to 15°, increasing depth estimate error by a factor of 2 to 3.

References

Biggar, G.M., O'Hara, M.J., Peckett, A., Humphries, D.J., 1971. Lunar lavas and the achondrites: petrogenesis of protohypersthene basalts in the maria lava lakes. Proceedings of the Lunar Science Conference 2, 617–643.

Brett, R., 1975. Thicknesses of some lunar mare basalt flows and ejecta blankets based on chemical kinetic data. Geochimica Cosmochimica Acta 39, 1135–1141.

Basaltic Volcanism Study Project, 1981. Section 5.4; Basaltic volcanism on the Moon. in: Basaltic Volcanism on the Terrestrial Planets, Lunar and Planetary Institute. Pergamon Press. New York, ISBN 0–08-028086-2, pp. 749–763.

Blewett, D.T., Coman, E.I., Hawke, B.R., GillisDavis, J.J., Purucker, M.E., Hughes, C.G., 2011. Lunar swirls: examining crustal magnetic anomalies and space weathering trends. Journal of Geophysical Research 116 http://dx.doi.org/10.1029/2010JE003656.

Carr, M.H., Greeley, R., 1980. Volcanic Features of Hawaii: A Basis for Comparison with Mars. 211 pp. NASA, SP-403. Washington, DC.

Coggins, J., Pratt, F., 1952. By Spaceship to the Moon. Random House, New York.

Coombs, C.R., Hawke, B.R., 1992. A Search for Intact Lave Tubes on the Moon: Possible Lunar Base Habitats. Paper Presented at The Second Conference on Lunar Bases and Space Activities of the 21st Century. NASA CP-3166. pp. 219–229.

Crawford, I.A., Fagents, S.A., Joy, K.H., 2007. Full Moon exploration: valuable (non-polar) lunar science facilitated by a return to the Moon. Astronomy and Geophysics 48 (3) 18-3.21.

Cushing, G.E., Titus, T.N., Wynne, J.J., Christensen, P.R., 2007. THEMIS observes possible cave skylights on Mars. Geophysical Research Letters 34, L17201, http://dx.doi.org/10.1029/2007Gl030709.

De Angelis, G., Wilson, J.W., Clowdsley, M.S., Nealy, J.E., Humes, D.H., Clem, J.M., 2002. Lunar lava tube radiation safety analysis. Journal of Radiation Research 43, S41–S45.

Gault, D.E., 1970. Saturation and equilibrium conditions for impact cratering on the lunar surface: criteria and implications. Radio Science 5, 273–291.

Gifford, A.W., El-Baz, F., 1981. Thicknesses of lunar mare flow fronts. Moon and Planets 24, 391–398.

Halliday, W.R., 1966. Terrestrial pseudokarst and the lunar topography. Bulletin of the National Speleological Society 28 (4), 167–170.

Halliday, W.R., 1998. "Pit craters," lava tubes, and open vertical conduits in Hawaii: A problem in terminology. Bulletin of the National Speleological Society 27B (1/4), 113–124.

Halliday, W.R., 2008. Differentiating Lava Tube Skylights from Pit Craters. A Study of the Cave-Like Structures on Arsia Mons, Mars. Geological Society of America Corilleran Section and Rocky Mountain Section Joint Meeting, 40. Abstract No. 1–2. p. 33.

Haruyama, J., Hioki, K., Shirao, K.M., Morota, T., Hiesinger, H., van der Bogert, C.H., Miyamoto, H., Iwasaki, A., Yokota, Y., Ohtake, M., Matsunaga, T., Hara, S., Nakanotani, S., Pieters, C.M., 2009. Possible lunar lava tube skylight observed by SELENE cameras. Geophysical Research Letters 36, L21206, http://dx.doi.org/10.1029/2009GL040635.

Haruyama, J., Hara, S., Hioki, K., Morota, T., Yokota, Y., Shirao, M., Hiesinger, H., van der Bogert, C.H., Miyamoto, H., Iwasaki, A., Ohtake, M., Saito, Y., Matsunaga, T., Nakanotani, S., Pieters, C.M., Lucey, P.G., 2010. New Discoveries of Lunar Holes in Mare Tranquillitatis and Mare Ingenii. Lunar Planetary Science Conference 41st (Abstract 1285).

Hatheway, A.W., Herring, A., 1970. Bandera lava tubes of New Mexico, and lunar implications, Communications of lunar and planetary laboratory. University of Arizona 8 (152), 299–327.

Heacock, R.L., Kuiper, G.P., Shoemaker, E.M., Urey, H.C., Whitaker, E.A., 1966. Ranger VIII and IX Part II. Experimenters' Analyses and Interpretations. JPL Technical Report 32–800.

Head III, J.W., 1976. Lunar volcanism in space and time. Review of Geophysics and Space Physics 14 (2), 265–300.

Head III, J.W., Wilson, L., 1992. Lunar mare volcanism: stratigraphy, eruption conditions and the evolution of secondary crusts. Geochimica Cosmochimica Acta 56, 2155–2175.

Hiesinger, H., Head III, J.W., Wolf, U., Jaumann, R., Neukum, G., 2002. Lunar mare basalt flow units: thickness determined from crater size-frequency distributions. Geophysical Research Letters 29, 1248, http://dx.doi.org/10.1029/2002GL014847.

Hiesinger, H., Head III, J.W., 2003. Ages and stratigraphy of mare basalts in Oceanus Procellarum, Mare Nubium, Mare Cognitum, and Mare Insularum. Journal of Geophysical Research 108 (E7), 5065, http://dx.doi.org/10.1029/2002JE001985.

Hiesinger, H., Head III, J.W., Wolf, U., Jaumann, R., Neukum, G., 2011. Ages and stratigraphy of lunar mare basalts: a synthesis. Geological Society of America SP-477, 1–51, http://dx.doi.org/10.1130/2011.2477(01).

Hood, L.L., Coleman Jr., P.J., Willhelms, D.E., 1979. Lunar nearside magnetic anomalies. Proceedings of Lunar Planetary Science Conference 10, 2235–2257.

Hörz, F., 1985. Lava Tubes: Potential Shelters for Habitats. in: Lunar bases and space activities of the 21st century (A86-30113 13-14). Lunar and Planetary Science Institute, Houston, TX, pp. 405–412.

Howard, K.A., 2010. Caldera collapse: perspectives from comparing Galápagos volcanoes, nuclear-test sinks, sandbox models, and volcanoes on Mars. GSA Today 20 (10), 4–10, http://dx.doi.org/10.1130/GSATG82A.1.

Howard, K.A., Head J.W.III, 1972. Regional Geology of Hadley Rille. in: Apollo 15: Preliminary Science Report. NASA SP-289. pp. 53–58.

Karlstrom, T.N.V., McCauley J.F., Swann G.A., 1968, Preliminary Lunar Exploration Plan of the Marius Hills Region of the Moon. United States Geological Survey. Interagency Report 5.

Kramer, G.Y., Combe, J.P., Harnett, E.M., Hawke, B.R., Noble, S.K., Blewett, D.T., McCord, T.B., Giguere, T.A., 2011. Characterization of lunar swirls at Mare Ingenii: a model for space weathering at magnetic anomalies. Journal of Geophysical Research, 116, http://dx.doi.org/10.1029/2010JE003669.

Kubo, N., Namiki, N., Ohtake, M., Yamaji, A., Haruyama, J., Matsunaga, T. 2010. Layering and Thickness of Basalitic Lava Flows in Mare Humorum: New Spectral Analysis of Multiband Imager Data of Kaguya (SELENE). Lunar Planetary Science Conference 41st (Abstract 1533).

Lloyd, D.D., Head III, J.W., 1972. Lunar surface properties as determined from earthshine and near-terminator photography. Geochimica Cosmochimica Acta Supplement 3, 3127–3142.

Masursky, H., Colton, G.W., El-Baz, F., 1978. Apollo Over the Moon: A View from Orbit. NASA. Washington, DC.

Nasmyth, J., Carpenter, J., 1885. The Moon: Considered as a Planet, a World, and a Satellite. London.

O'hara, M.J., Biggar, G.M., Richardson, S.W., Ford, C.E., Jamieson, B.G., 1970. The nature of seas, mascons and the lunar interior in the light of experimental studies. Geochimica Cosmochimica Acta, Supplement 1. Proceedings of the Apollo 11 Lunar Science Conference, Houston, TX. New York: Pergammon Press, pp. 695–710.

Okubo, C.H., Martel, S.J., 1998. Pit crater formation on Kilauea volcano, Hawaii. Journal of Volcanological and Geothermal Research 86, 1–18.

Robinson, M.S., Brylow, S.M., Tschimmel, M., Humm, D., Lawrence, S.J., Thomas, P.C., Denevi, B.W., Bowman-Cisneros, E., Zerr, J., Ravine, M.A., Caplinger, M.A., Ghaemi, F.T., Schaffner, J.A., Malin, M.C., Mahanti, P., Bartels, A., Anderson, J., Tran, T.N., Eliason, E.M., McEwen, A.S., Turtle, E., Jolliff, B.L., Hiesinger, H., 2010. Lunar Reconnaissance Orbiter Camera (LROC) instrument overview. Space Science Review 150 (1–4), 81–124.

Schaber, G.G., 1973. Eratosthenian Volcanism in Mare Imbrium: Source of Youngest Flows. in: Apollo 17: Preliminary Science Report. NASA SP-330. pp. 30-17–30-25.

Schaber, G.G., Boyce, J., Moore, H.J., 1976. The scarcity of mappable flow lobes on the lunar maria: unique morphology of the imbrium flows. Proceedings of the Lunar Science Conference 7, 2783–2800.

Sharpton, V.L., Head III, J.W., 1982. Stratigraphy and structural evolution of southern Mare Serenitatis: a reinterpretation based on Apollo Lunar Sounder Experiment data. Journal of Geophysical Research 87 (B13) 10,983–10,998.

Shearer, C.K., Hess, P.C., Wieczorek, M.A., Pritchard, M.E., Weiss, B.P., Williams, J.G., Hood, L.L., Righter, K., Neal, C.R., Shearer, C.K., McCallum, I.S., Tompkins, S., Hawke, B.R., Peterson, C., Gillis, J.J., Bussey, B., 2006. Thermal and magmatic evolution of the Moon. Review of Mineralogical Geochemistry 60, 365–518.

Spudis, P.D., Swann, G.A., Greeley, R., 1988. The formation of Hadley Rille and implications for the geology of the Apollo 15 region. Proceedings of the Lunar Planetary Science Conference 18, 243–254.

Spudis, P.D., McGovern, P.J. Kiefer, W.S., 2011, Large Shield Volcanoes on the Moon. in Lunar Planetary Science Conference. Abstract 42, Abstract 1367.
Tran, T.N., Roseik, M.R., Beyer, R.A., Mattson, S., Howington-Kraus, E., Robinson, M.S., Archinal, B.A., Edmundson, K., Harbour, E., Anderson, E., LROC Science Team. 2010. Generating digital terrain models using LROC NAC images. in: ISPRS Technical Commission IV & AutoCarto. Orlando, FL. p. 7.
Weider, S.Z., Crawford, I.A., Joy, K.H., 2010. Individual lava flow thicknesses in Oceanus Procellarum and Mare Serenitatis determined from Clementine multispectral data. Icarus 209 (2), 323–336.
Whitford-Stark, J.L., Head, J.W., 1977. The Procellarum volcanic complexes—contrasting styles of volcanism. Proceedings of Lunar Planetary Science Confernce 8, 2705–2724.
Whitaker, E.A., 1972, Mare Imbrium Lava Flows and Their Relationship to Color Boundaries. in: Apollo 15: Preliminary Science Report. NASA Spec. Pub. 289, pp. 83-84.
Wilhelms, D.E., 1972. Geologic Map of the Taruntius Quadrangle of the Moon. Map I-722. U.S. Geological Survey. Department of the Interior. Flagstaff, AZ.